applied sciences

MDPI

Article

Polyethylene Terephthalate Fiber Modified with Type I Collagen as a 3D Scaffold Material for Bioartificial Liver

Yang Li [1,2,3], Yang Zhang [1], Jianping Gao [1,2], Shuguang Liao [3] and Guifeng Zhang [1,2,*]

[1] National Key Laboratory of Biochemical Engineering, Institute of Process Engineering, Chinese Academy of Sciences, Beijing 100190, China; liyang2343@163.com (Y.L.); zhangyang21@ipe.ac.cn (Y.Z.); jpgao@ipe.ac.cn (J.G.)
[2] School of Chemical and Engineering, University of Chinese Academy of Sciences, Beijing 100049, China
[3] Institute of Regenerative Medicine, Zhujiang Hospital, Southern Medical University, Guangzhou 510280, China; xiaoliao0803@126.com
* Correspondence: gfzhang@ipe.ac.cn

Abstract: Acute and chronic liver failure are clinically significant conditions, and the artificial liver support system (ALSS) is emerging as a novel and effective approach for the clinical management of liver failure. Within this framework, scaffold materials occupy a pivotal position as integral components of the bioreactor. Elevating the performance capabilities of these scaffolds not only augments the therapeutic efficacy of the artificial liver but also lays the groundwork for refining and selecting large-scale hepatocyte culture models. In this study, we introduced a novel hepatocyte scaffold material designated as PET-COL, crafted by coating polyethylene terephthalate (PET) with collagen. This involved a sequence of modifications, including alkaline hydrolysis, EDC/NHS activation and crosslinking, as well as collagen conjugation. The physicochemical attributes of the scaffold were thoroughly characterized by Fourier-transform infrared spectroscopy (FTIR), X-ray photoelectron spectroscopy (XPS), second harmonic generation (SHG), water contact angle measurements, and high-performance liquid chromatography–mass spectrometry (HPLC-MS). Furthermore, an investigation into the material's biological properties was conducted that encompassed SEM (HepaRG growth), fluorescence staining (assessment of cell viability), staining by trypan blue (HepaRG counting), CCK-8 (proliferation of cells), biochemical testing, and immunosorbent assay. Our findings revealed that collagen was covalently bonded to the PET surface, leading to a substantial enhancement in the material's hydrophilicity ($p < 0.001$). The quantity of collagen coating was determined to be precisely 33.30 μg per scaffold. Human liver progenitor HepaRG cells thrived on the PET-COL material. Compared with the untreated group, cell viability, albumin secretion, urea synthesis, and the expression levels of CYP3A4 and CPS1 increased significantly ($p < 0.001$), demonstrating remarkable biological vitality. The PET-COL scaffold, as developed in this study, holds immense potential for application in bioartificial livers.

Keywords: PET; type I collagen; bioartificial liver; three-dimensional culture; scaffold materials; surface modification; progenitor cells; hepatocytes

Citation: Li, Y.; Zhang, Y.; Gao, J.; Liao, S.; Zhang, G. Polyethylene Terephthalate Fiber Modified with Type I Collagen as a 3D Scaffold Material for Bioartificial Liver. *Appl. Sci.* **2024**, *14*, 4537. https://doi.org/10.3390/app14114537

Academic Editors: Dorota Korte and Mohanachandran Nair Sindhu Swapna

Received: 24 April 2024
Revised: 17 May 2024
Accepted: 22 May 2024
Published: 25 May 2024

1. Introduction

Liver failure is a severe illness characterized by liver dysfunction, often resulting from viruses [1], alcohol abuse [2], drug exposure [3], and other factors. It is marked by significant morbidity and mortality rates [4,5]. The primary pathological alteration in liver failure is the widespread death of liver cells, which are challenging to regenerate, thus compromising the liver's ability to efficiently carry out its vital functions of synthesis, transformation, and detoxification; consequently, this can trigger a cascade of critical health complications, including jaundice, hepatic encephalopathy, and coagulation disorders [6,7]. Presently, liver transplantation stands as the definitive treatment for patients with liver

failure; however, the acute shortage of donor livers poses a significant limitation to the widespread clinical application of this procedure [8,9].

Research on artificial liver technology holds significant importance in refining and improving the ongoing treatment of patients suffering from liver function failure [10–12]. Among various technologies, the bioartificial liver stands out as an extracorporeal biological reaction system grounded in hepatocytes. Its mechanism involves cultivating hepatocytes in an external circulation device, referred to as a bioreactor, where a substance exchange takes place between the hepatocytes and the patient's plasma either through a semi-permeable membrane or direct contact, thereby aiding liver function. When juxtaposed with mechanical artificial livers [13], the bioartificial liver offers not just detoxification abilities but also carries out synthetic metabolism and biotransformation functions within the bioreactor, thus providing a more holistic liver function replacement [14,15]. Ensuring a high-density, large-scale hepatocyte culture within the bioreactor while preserving its viability and function is pivotal for amplifying the therapeutic effectiveness of bioartificial livers [16–18]. Tissue-engineered three-dimensional cultures represent the evolving trend in artificial liver bioreactor technology [19,20]. Given that hepatocytes are polarized, anchorage-dependent cells that naturally proliferate within a three-dimensional network scaffold composed of diverse extracellular matrices in vivo, mimicking this native environment through the preparation of a three-dimensional porous scaffold could potentially facilitate tissue-engineered three-dimensional culture in vitro.

Polyethylene terephthalate (PET) is a condensation polymer derived from terephthalic acid and ethylene glycol. As a synthetic polymer biomaterial, PET demonstrates remarkable mechanical strength, corrosion resistance, heat tolerance, and optical properties. Easily modifiable and processable, its application in the fields of biology and medicine is expanding rapidly [21,22]. Despite PET's good chemical stability in body fluids [23], its pronounced hydrophobicity, stemming from chemical inertness, absence of polar groups, and low surface energy, significantly impacts its biocompatibility. PET's inability to induce tissue remodeling limits its capacity to enhance cell functionality and activity in in vitro cultures [24].

Collagen is the main component of the extracellular matrix (ECM), which can self-assemble into cross-striped fibers, providing support for cell growth and giving connective tissue a certain mechanical toughness [25]. Collagen has many important biological characteristics, for example, it can serve as a substrate for cell adhesion and migration, providing signals to cells to regulate their functions; it can form three-dimensional scaffolds of various physical configurations to support cell growth and construct engineered tissues; it can also be enzymatically degraded in the body with low immune rejection, which is beneficial for tissue regeneration and repair. In addition, it is abundant in sources, easy to extract, and low cost. These characteristics make collagen the main natural biological raw material for constructing tissue engineering scaffolds. As a bioactive material, collagen has the advantages of biocompatibility, biodegradability, cell adhesion, and low immunogenicity; however, compared to synthetic polymer materials, it lacks certain mechanical strength and stability. Although the plasticity of collagen allows people to develop different forms of in vitro controllable assembly materials for different clinical diseases [26–28], its mechanical strength and stability still cannot meet the basic requirements of cell culture scaffolds that respond to fluid shear forces in bioartificial liver reactors.

Chemical crosslinking is an important polymer material modification process that involves connecting macromolecular chains (such as polymers) through chemical bonds under various factors such as light, heat, high-energy radiation, mechanical force, ultrasound, or crosslinking agents, thereby constructing a reticulated or specifically structured polymer material. In the biological field, chemical crosslinking is also used to link proteins to study the interaction between proteins and proteins, as well as between proteins and solid phases. Currently, common crosslinking agents for collagen chemical crosslinking modification include aldehydes [29], carbodiimides (EDC), polycarboxylic acid-N-hydroxysuccinimide (NHS) esters, and diepoxy substances. Among them, glutaraldehyde is a commonly used

chemical reagent for collagen crosslinking but it has certain cytotoxicity [30] and is not suitable for the development of medical device products. As a zero-length crosslinking agent, EDC can activate carboxyl groups and is often used in conjunction with NHS as a catalyst for crosslinking reactions between proteins. It has the advantages of high efficiency, safety, and non-toxicity. In addition, studies have found that collagen scaffolds crosslinked with EDC/NHS exhibit superior stability and cell compatibility [31].

Based on the key components of the extracellular matrix and the characteristics of the hepatocyte growth microenvironment, this study used chemical modification methods to hydrolyze the ester groups on the PET surface to expose carboxyl groups, followed by EDC/NHS-activated crosslinking, collagen coupling, and reactive-group blocking treatment to construct type I collagen-coated PET fibrous scaffolds. The physicochemical properties of the scaffolds were characterized, including surface functional group structure, chemical element composition, hydrophilicity, and collagen coating content. Through HepaRG cell culture experiments, the biological performance of the material, including cell adhesion and cell proliferation activity, was further studied to evaluate the impact of the scaffolds on hepatocyte growth and metabolic activities, thereby demonstrating their potential application in artificial liver support systems.

2. Materials and Methods

2.1. Materials

The PET fiber scaffolds, which were of medical grade and commercially available, were cut into sheets of similar size (2.0 cm × 0.6 cm × 0.3 cm). Bovine Achilles tendon type I collagen was obtained from Hebei Collagen Biotechnology Co., Ltd. (Handan, China); NaOH was purchased from Tianjin Damao Chemical Reagents Factory (Tianjin, China); 1-Ethyl-3-(3-dimethylaminopropyl) carbodiimide (EDC) was purchased from Tokyo Chemical Industry (Tokyo, Japan); N-hydroxysuccinimide (NHS) was purchased from Shanghai Aladdin Biochemical Technology Co., Ltd. (Shanghai, China); 2-(4-morpholino) ethanesulfonic acid (MES) and lysine were purchased from Beijing Xin Jing Ke Biotechnology Co., Ltd. (Beijing, China); other analytical-grade chemical reagents like ethanol and acetone were purchased from Beijing Chemical Works (Beijing, China).

2.2. Preparation of the Materials

2.2.1. The Scheme of Collagen Immobilization

The collagen-coated three-dimensional polyester fiber scaffold, designated as PET-COL, was fabricated according to the subsequent steps. Initially, the PET fiber scaffold underwent treatment with a NaOH solution to hydrolyze the ester groups, thereby revealing the carboxyl groups (denoted as PET-COO). Subsequently, EDC and NHS were introduced to produce a semi-stable amine-reactive NHS ester with the carboxyl groups (labeled as PET-NHS), facilitating additional crosslinking reactions. Ultimately, a durable amide bond was established between PET-NHS and collagen (Figure 1).

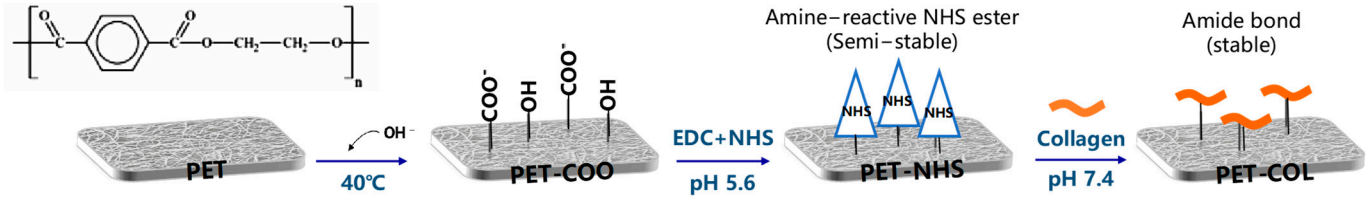

Figure 1. The scheme of collagen immobilization on the surface of three-dimensional polyester fiber scaffold.

2.2.2. Modification by NaOH

Before modification, the PET fiber scaffolds underwent separate washes for 10 min each in ethanol, acetone, and distilled water, all while undergoing ultrasonication treatment. Following this, the scaffolds were placed in a 5% NaOH solution at 40 °C for 40 min

to hydrolyze and break the ester groups, thereby exposing the carboxyl groups (PET-COO). Afterward, the PET-COO scaffolds were washed thoroughly with deionized water and dried.

2.2.3. Collagen Immobilization

The PET-COO fiber scaffolds were immersed in a 0.1 M MES solution (pH = 5.6) for 1 h. Subsequently, 2 mM EDC and 6 mM NHS were added to the MES solution at 25 °C for 30 min to facilitate further activation and crosslinking reactions (PET-NHS). Subsequently, the PET-NHS scaffolds were washed with ultrapure water.

Type I collagen was dissolved in acetic acid to prepare a solution with a concentration of 5 mg/mL. The pH of the collagen solution was adjusted to 7.2–7.5 using sodium hydroxide. The scaffolds were then added to the collagen solution and incubated at 25 °C for 2 h to allow for coupling. The scaffolds were washed five times with ultrapure water for 10 min each. After washing with deionized water, the scaffolds were placed in a 10 mg/mL lysine solution at 25 °C for 2 h to block the active groups (PET-COL). Finally, the fiber scaffolds were washed again with deionized water and dried using an air blast.

2.3. Surface Characterization

2.3.1. X-ray Photoelectron Spectroscopy (XPS)

The composition and structure of the surface layer on the scaffolds were analyzed using an X-ray photoelectron spectroscope spectrometer (ESCALAB 250Xi, Thermo Fisher Scientific, Waltham, MA, USA) equipped with a monochromatic Al Kα X-ray source (energy of 1486.6 eV). The analysis was conducted under the following conditions: 225 W power (12 kV voltage, 15 mA current), with a minimum energy resolution of 0.48 eV (Ag3d5/2). The C1s, N1s, and O1s spectra were collected over a binding energy range of 0–1350 eV with a step size of 1 eV.

2.3.2. Fourier-Transform Infrared Spectroscopy

The Fourier-transform infrared (FTIR) spectra of PET, PET-COO, and PET-COL were acquired using a NICOLET iS50 FT-IR spectrometer (Thermo Fisher Scientific, Waltham, MA, USA). The analysis was conducted in transmittivity mode, covering the spectral range of 1200 cm^{-1} to 3600 cm^{-1} with a resolution of 4 cm^{-1}. Each spectrum was collected by averaging 32 scans.

2.3.3. Water Contact Angle

The surface wettability of PET, PET-COO, and PET-COL was evaluated using a contact angle goniometer (K100, Kruss, Hamburg, Germany). A droplet volume of 2 µL was used, and the contact angles were measured at 0 s, 5 s, and 10 s after placing the water droplets on the surface of the samples. Each group of samples was measured three times.

2.3.4. Second Harmonic Generation Imaging (SHG)

Second harmonic generation is a microscopy technique used to study nonlinear optical effects, often applied to observe the structure of molecules such as collagen. The scaffold materials were made into paraffin sections, and SHG signals were collected using two-photon confocal microscopy (TCS SP5, Leica, Wetzlar, Germany). The excitation wavelength was set to 880 nm to observe the collagen coupling on the scaffolds.

2.3.5. Detection of Collagen Coating Content by High-Performance Liquid Chromatography Mass Spectrometry

Utilizing HPLC-MS technology, we proceeded to assess the hydroxyproline content present on the surface of PET fibers subsequent to the application of a Type I collagen coating. Collagen is composed of 18 amino acids, of which hydroxyproline is one of the characteristic amino acids of collagen. Its content in collagen is relatively constant, about

12%. Based on this, the content of collagen can be indirectly calculated by measuring the content of hydroxyproline.

To detect the content of collagen coating on the scaffold samples, 10 mg of the samples were weighed and added to 6 M HCl at 110 °C for 24 h of hydrolysis. After cooling and drying, the samples were re-dissolved in 1 mL of ultrapure water. Hydroxyproline was used as the standard, and the concentration of hydroxyproline was detected by high-performance liquid chromatography (UltiMate 3000 RS, Thermo Fisher Scientific, Waltham, MA, USA) coupled with mass spectrometry (TSQ QUANTUM ACCESS MAX, Thermo Fisher Scientific, Waltham, MA, USA), which indirectly determined the content of collagen in the sample.

The hydroxyproline concentration (A) was calculated by plotting data points on a standard curve with the area of the HPLC peak on the Y-axis and the hydroxyproline concentration on the X-axis. The amount of type I collagen (m) in the sample can be calculated using the formula below, where V represents the volume of the sample after post-hydrolysis resuspension, and D represents the dilution ratio of the sample.

$$m = \frac{A \times V \times D}{12\%} \quad (1)$$

2.4. Cell Culture

2.4.1. Culture of HepaRG Cells on the Scaffolds

The scaffolds (2.0 cm × 0.6 cm × 0.3 cm), sterilized using electron beam radiation, were placed in 12-well plates (BIOFIL, Guangzhou, China). HepaRG cells were purchased from Biopredic International (Rennes, France) and were cultured in William's E Medium (Thermo Fisher Scientific, Waltham, MA, USA) supplemented with Metabolism Medium Supplement (Thermo Fisher Scientific, Waltham, MA, USA) at 37 °C in a CO_2 incubator (MCO-20AIC, SANYO, Osaka, Japan). HepaRG cells in the logarithmic growth phase were prepared as a cell suspension and inoculated into the scaffolds at a concentration of 2×10^6 cells/mL. The culture medium was refreshed every other day.

2.4.2. Scanning Electron Microscopy (SEM) Analysis

After 1, 3, 5, and 8 days of cell culture, scanning electron microscopy (SEM, JEOL JSM-6700F, Akishima, Japan) was used to observe and compare the morphological differences between HepaRG cells grown on PET and PET-COL scaffolds. The scaffolds were first washed three times using phosphate buffer saline (PBS), then fixed with 2.5% glutaraldehyde at 4 °C overnight. Subsequently, the scaffolds were dehydrated using a gradient ethanol wash for 15 min each at room temperature. Finally, the scaffolds were dried using CO_2 critical point drying (K850, Quorum, Brighton, UK) and sputter-coated with platinum (JFC1600, JEOL, Akishima, Japan). The samples were then observed and photographed under a JSM-6700F scanning electron microscope (JEOL, Akishima, Japan).

2.4.3. Fluorescence-Based Viability Staining

To investigate the viability of HepaRG cells grown on PET and PET-COL scaffolds, a Live–Dead Cell Staining kit (KeyGEN BioTECH, Nanjing, China) was utilized to stain the cells. The supernatant of the samples was removed, and the samples were washed three times with PBS. Subsequently, 500 μL of staining solution—a mixture of 1 μL of calcein (AM) and 1 μL of propidium iodide (PI) in 1 mL of PBS—was added, and the HepaRG cells cultured on scaffolds were incubated at room temperature for 30 min. After removing the staining solution, 500 μL of fluorescent mounting media (Beyotime Biotechnology, Shanghai, China) was added, and fluorescence was observed and photographed under an inverted fluorescence microscope (Axio Vert A1, ZEISS, Oberkochen, Germany).

2.4.4. Cell Counting

To investigate the viability of HepaRG cells grown on PET and PET-COL scaffolds, the supernatant of the samples in the culture plate was first removed, and the samples were

then washed three times with PBS. Subsequently, lysis buffer (Reagent A100, Chemometec, Allerod, Danmark) containing 0.04% trypan blue staining solution (Leagene, Beijing, China) was added onto scaffolds and incubated at room temperature for 5 min. The lysis buffer was used to lyse the membrane of the cells adhered to the scaffolds, releasing the nuclei, which could be stained by trypan blue. Finally, a blood counting chamber was utilized to count the cell nuclei.

2.4.5. CCK-8 Assay

To assess cell proliferation, the Cell Counting Kit-8 (CCK-8, Biosharp, Hefei, China) was used (n = 3). Following the removal of the culture medium, samples underwent three washes with PBS. Subsequently, 150 µL of CCK-8 solution was added to each well and incubated at 37 °C for 3 h. After incubation, 90 µL of the solution was transferred to a 96-well plate (BIOFIL, Guangzhou, China), and the optical density (OD) was measured at 450 nm using a microplate reader (Multiskan GO, Thermo Fisher Scientific, Waltham, MA, USA).

2.4.6. Biochemical Testing

To evaluate the conversion of ammonia to urea by HepaRG cells grown on PET and PET-COL scaffolds, the supernatant from the same time points as described above was substituted with complete medium containing 3 mM NH_4Cl. The medium was then incubated in a carbon dioxide incubator for 90 min. After incubation, the medium was collected for the assay of urea synthesis.

2.4.7. Enzyme-Linked Immunosorbent Assay (ELISA)

Albumin (ALB), carbamyl phosphate synthase1 (CPS1), and cytochrome P450 3A4 (CYP3A4) in HepaRG cells were detected using a Human ELISA kit (Jiangsu Meimian Industrial Co., Ltd., Yancheng, China). Samples for detecting ALB were obtained from the culture supernatant at different time points (1, 3, 5, and 8 days), while samples for detecting CYP3A4 and CPS1 were obtained from the cell lysate using a repetitive freeze–thaw method. The OD of each sample was measured at 450 nm.

2.5. Statistical Analysis

All of the quantitative data are presented as mean ± standard deviation. Statistical analyses were performed using *t*-tests; *p*-values less than 0.05 were considered statistically significant.

3. Results and Discussion

3.1. Surface Characterization

3.1.1. X-ray Photoelectron Spectroscopy (XPS)

Polyethylene terephthalate (PET) has the chemical formula $(C_{10}H_8O_4)_n$, and is composed of carbon, hydrogen, and oxygen. To investigate the fibrous surface modification process, we employed the XPS technique, which is capable of detecting all elements except hydrogen and helium. In PET and PET-COO, we observed signals with binding energies of 292.4 eV and 537.3 eV, representing the presence of C1s and O1s, respectively (Figure 2). Following type I collagen modification, the XPS spectrum of PET-COL exhibited an induced N1s signal at 404.45 eV, indicating the introduction of nitrogen (N), an element undetectable in PET and PET-COO. Furthermore, the elemental composition analysis (Table 1) revealed that, compared to PET, the C content in PET-COL after collagen coating decreased from 71.34% to 62.78%, while the O content decreased from 27.91% to 19.47%. Notably, the N content reached 17.36%. XPS results further confirmed that crosslinking modification of PET with collagen successfully introduced nitrogen-containing groups onto the material surface, indicating that collagen had been effectively coated onto the PET fiber scaffold surface through the aforementioned step-by-step manipulations.

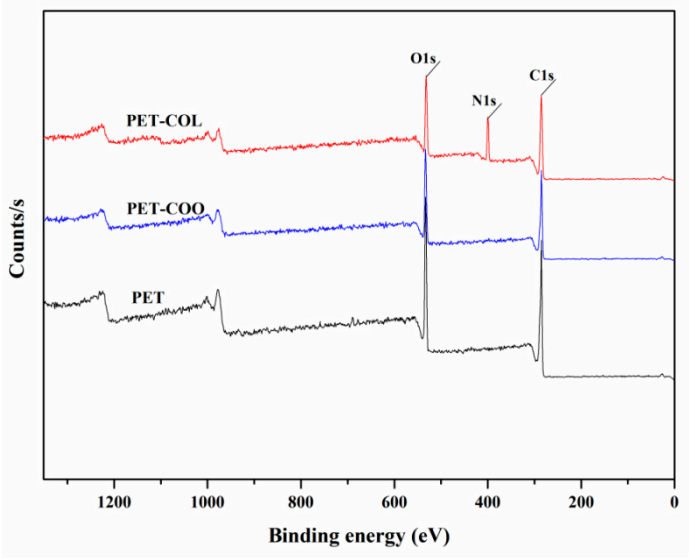

Figure 2. The XPS scan spectra of PET, PET-COO, and PET-COL scaffolds.

Table 1. Surface elementary composition of the scaffolds from XPS analysis.

Sample	Elementary Composition		
	C (%)	N (%)	O (%)
PET	71.34	0.47	27.91
PET-COO	71.96	0.89	26.74
PET-COL	62.78	17.36	19.47

3.1.2. Fourier-Transform Infrared Spectroscopy

The molecular structure of PET material abundantly features ester groups. When exposed to an alkaline environment, hydroxide ions (OH-) proactively engage in nucleophilic addition reactions with the carbonyl carbon (C=O) present in the ester bond. This interaction leads to the hydrolysis of the ester bond, giving rise to carboxyl groups (-COOH) and hydroxyl groups (-OH) [32]. These newly formed polar functional groups offer reactive sites for subsequent chemical modifications on the material, thereby expanding its potential applications in biomedical fields. Referring to Figure 3, we noticed that, in comparison to PET, PET-COO—following the hydrolysis of ester groups—exhibits a prominent hydroxyl characteristic absorption peak at 3430 cm^{-1}. This finding suggests the successful introduction of hydroxyl groups onto the material's surface. Nevertheless, no appreciable alterations were detected at the characteristic absorption peak corresponding to carboxyl groups in PET-COO. This observation could be attributed to the fact that the emergence of carboxyl groups primarily stems from the internal cleavage of ester groups. Given that the infrared spectra of both ester and carboxyl groups are predominantly influenced by the stretching vibration of C=O, distinguishing them spectroscopically poses a challenge. Consequently, we can indirectly ascertain the occurrence of a hydrolysis reaction on the PET material's surface by scrutinizing the characteristic absorption peak of hydroxyl groups. Referring again to Figure 3, subsequent to EDC/NHS activation and crosslinking with collagen, PET-COL displays distinct absorption peaks corresponding to Amid II, Amid I, and Amid A of type I collagen at 1550 cm^{-1}, 1665 cm^{-1}, and 3330 cm^{-1}, respectively. This provides compelling evidence that collagen has been covalently grafted onto the PET material's surface.

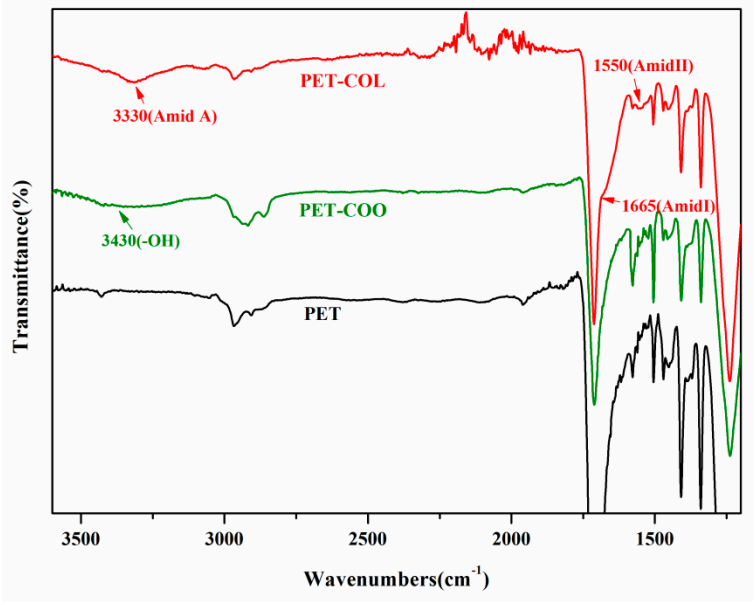

Figure 3. FTIR infrared spectrum of PET, PET-COO, and PET-COL scaffolds.

3.1.3. Water Contact Angle

Hydrophilicity serves as a crucial indicator for assessing the biocompatibility of materials, making it highly relevant for biomedical applications [33–35]. This biocompatibility can be effectively evaluated by measuring the water contact angle of the materials. Figure 4A illustrates the water contact angle measurements for PET, PET-COO, and PET-COL at 0 s, 5 s, and 10 s.

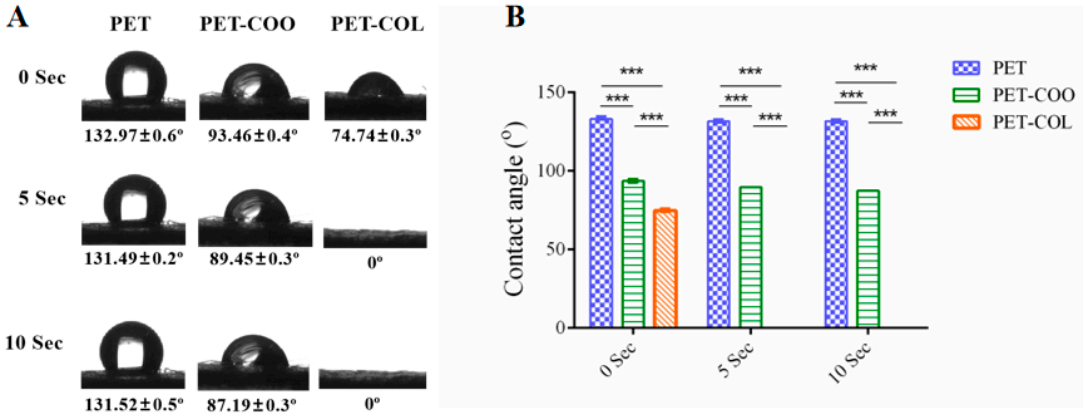

Figure 4. Water contact angle of PET, PET-COO, and PET-COL scaffolds. (**A**): The change in water contact angle at three time points (0 s, 5 s, and 10 s); (**B**): the statistical histogram of water contact angle in different samples at three time points (0 s, 5 s, and 10 s). Data are mean ± SD, n = 3; ***: $p < 0.001$.

The results reveal that the water contact angles for untreated PET at 0 s, 5 s, and 10 s were 132.97 ± 0.6°, 131.49 ± 0.2°, and 131.52 ± 0.5°, respectively. Following strong alkaline hydrolysis, the water contact angles for PET-COO decreased significantly to 93.46 ± 0.4°, 89.45 ± 0.3°, and 87.19 ± 0.3° at 0 s, 5 s, and 10 s, respectively, when compared to PET ($p < 0.001$) (Figure 4B). These findings suggest that strong alkaline hydrolysis effectively alters the hydrophilicity of PET materials, leading to improved wettability.

When considered alongside the results obtained from FTIR analysis in Section 3.2.2, it is plausible that the hydrolysis reaction of ester groups on the material's surface gives rise to the formation of hydrophilic -OH groups, thereby enhancing the surface hydrophilicity of the material. Upon coating with type I collagen, the water contact angles for PET-COL

further diminished to 74.74 ± 0.3°, 0°, and 0° at 0 s, 5 s, and 10 s, respectively (Figure 4A). These reductions were statistically significant when compared to both PET and PET-COO ($p < 0.001$) (Figure 4B). Evidently, collagen coating further enhances the hydrophilicity of PET materials.

3.1.4. Second Harmonic Generation Imaging (SHG)

Figure 5 illustrates the second harmonic signal image of PET fibers coated with Type I collagen. The PET-COL surface demonstrates a consistently dense green fluorescent signal, signifying the even distribution of collagen, while the PET surface remains devoid of any fluorescent signal. This provides additional evidence that collagen has been evenly applied to the PET surface.

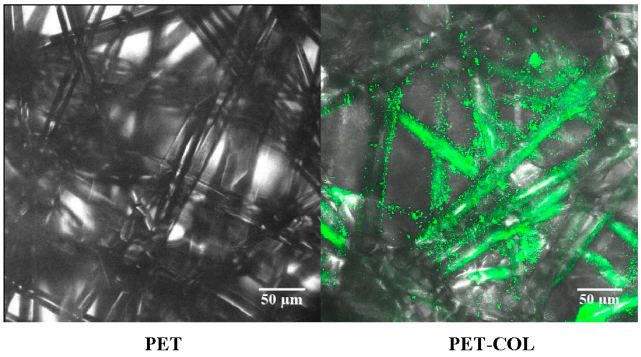

Figure 5. SHG images of PET and PET-COL scaffolds. Scale bar: 50 μm.

3.1.5. Detection of Collagen Coating Content by HPLC-MS

Through the incorporation of the HPLC-MS results pertaining to PET-COL (Figure 6B) into the hydroxyproline standard curve function (Figure 6A), coupled with the implementation of the formula outlined in Section 2.3.5, we have determined that the collagen content of PET-COL amounts to 33.30 μg/piece.

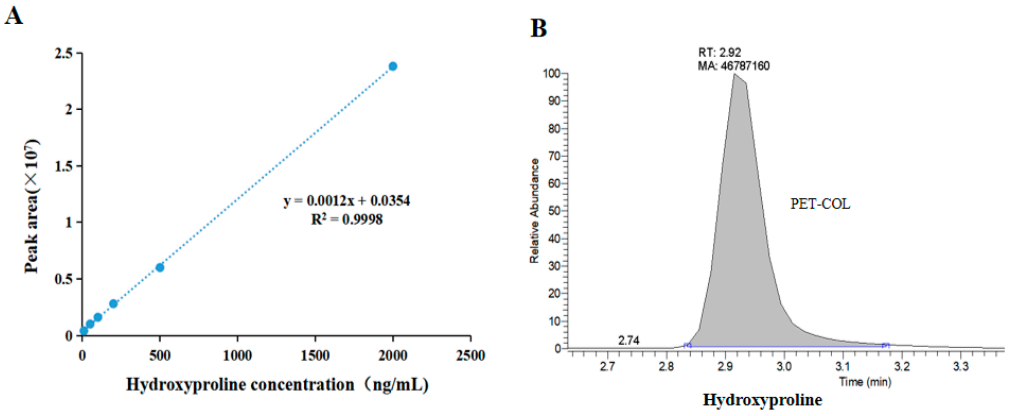

Figure 6. Hydroxyproline content on PET fibers after type I collagen coating. (**A**): Standard curve of Hydroxyproline; (**B**): Hydroxyproline peak graph of PET-COL surface.

3.2. Cell Culture

3.2.1. Cell Morphology

The growth of HepaRG cells on PET and PET-COL scaffolds was observed using a cold-field emission scanning electron microscope (refer to Figure 7). The findings indicated that, on the first day of incubation, cells could be seen adhering to and accumulating on the surface of the PET-COL fibers. As incubation progressed, the cell population on the PET-COL fibers increased significantly, eventually leading to the formation of cellular clusters by the fifth day, displaying a three-dimensional organizational structure. This implies that

PET-COL can create a favorable environment for cell growth, promoting cell adhesion and proliferation. In contrast, cell growth on PET fibers remained minimal, highlighting its restrictions in supporting cell development.

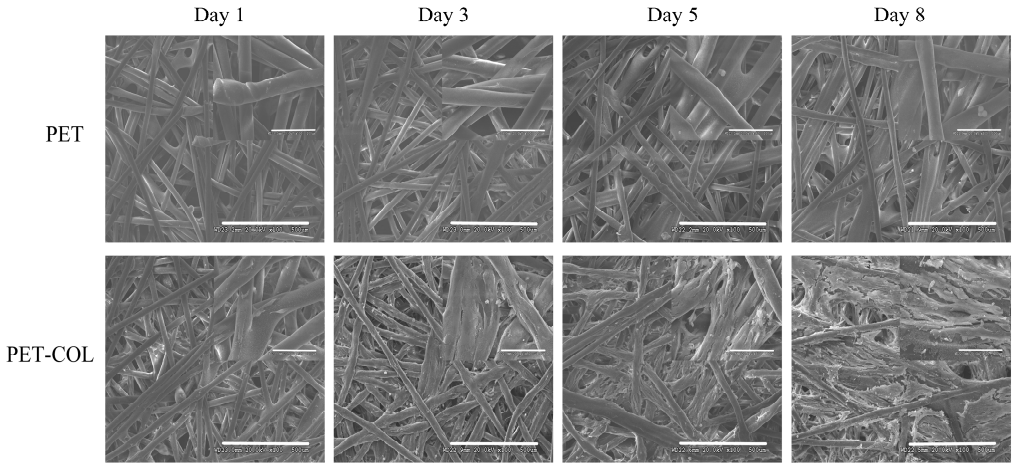

Figure 7. SEM photographs of HepaRG cells growing on PET and PET-COL fibers, taken on day 1, day 3, day 5, and day 8. Scale bar: 500 μm.

3.2.2. Cell Viability

Utilizing fluorescent staining for cell viability assessment allows us to visually evaluate the activity status of HepaRG cells cultured on PET and PET-COL fiber scaffolds. The results presented in Figure 8 demonstrate that as the culture duration increases, PET-COL scaffolds show a gradual enhancement in green fluorescent signals, signifying live cells, in terms of both intensity and quantity. This trend suggests that PET-COL scaffolds effectively support cell growth and proliferation, thereby offering a conducive environment for cell development. Conversely, on PET scaffolds, predominantly red fluorescent signals, indicative of dead cells, are observed, with scarcely any visible green fluorescence. This finding implies that PET scaffolds offer limited support for cell growth, leading to reduced cell activity and a higher cell death rate.

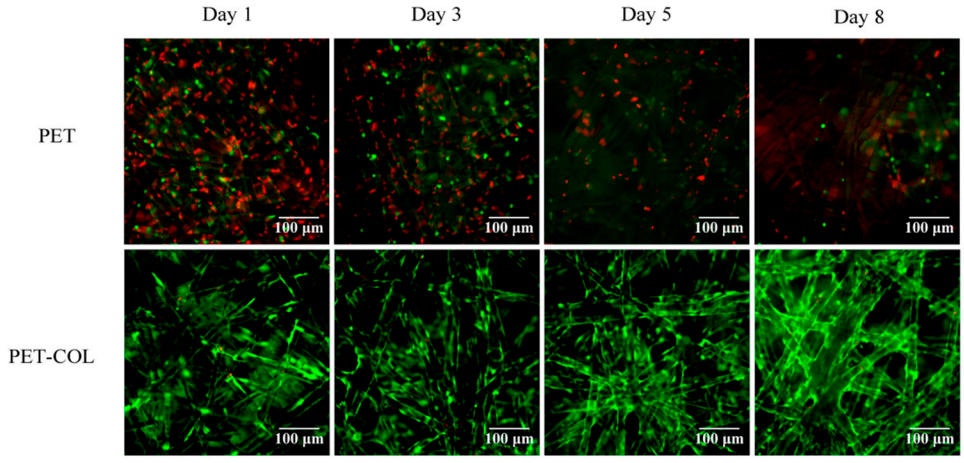

Figure 8. Live–dead fluorescence staining photographs of HepaRG cells growing on PET and PET-COL fibers, taken on day 1, day 3, day 5, and day 8. Scale bar: 100 μm.

3.2.3. Cell Proliferation

Cell counting and CCK-8 assays were performed on HepaRG cells cultivated on PET and PET-COL scaffolds at culture days 1, 3, 5, and 8 to evaluate the impact of these materials on cell proliferation and viability. The findings revealed that as the duration of

culture progressed, the cell count on the PET-COL scaffolds demonstrated a steady increase (Figure 9A), paralleled by a corresponding rise in OD450 nm absorbance (Figure 9B). In contrast, the PET scaffolds demonstrated notably lower values for both metrics in comparison to PET-COL, with significant statistical differences between the two. These findings indicate that the collagen coating is more conducive to enhancing HepaRG cell proliferation and maintaining cell viability.

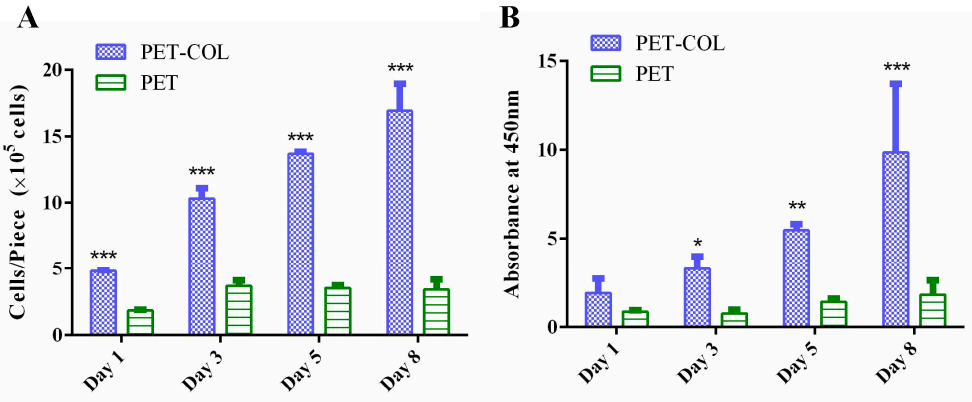

Figure 9. Proliferation of HepaRG cells growing on PET and PET-COL fibers on day 1, day 3, day 5, and day 8. (**A**) Cell counting results; (**B**) CCK-8 results. Data are mean ± SD, n = 3; *: $p < 0.05$, **: $p < 0.01$, ***: $p < 0.001$.

3.2.4. Cell Function

The clinical significance of the liver primarily lies in its two vital functions: synthesis and detoxification via biochemical transformations. In cases of liver failure, patients often encounter various complications stemming from an inability to synthesize plasma proteins and detoxify harmful substances. Among these complications, ammonia accumulation-induced hepatic encephalopathy is the most prevalent. HepaRG is classified as a type of human liver progenitor cell. Because of its high expression of liver functions, including drug metabolism-related enzymes, urea synthesis, and transporter proteins, as well as its similarity to primary human hepatocytes, it is currently a widely recognized cell model [36,37]. Additionally, HepaRG cells exhibit bipotential differentiation capacity and can differentiate into mature hepatocytes or cholangiocytes under specific culture conditions. Research has revealed that extracellular matrix components can regulate the differentiation of HepaRG cells [38–40]. To further assess the functional performance of HepaRG cells cultured on PET and PET-COL scaffolds, we analyzed the levels of albumin and urea present in the cell culture supernatant. Our findings revealed that as the duration of cell culture progressed, both the albumin secretion (Figure 10A) and urea synthesis (Figure 10B) abilities of HepaRG cells cultivated on PET-COL scaffolds exhibited a gradual upward trajectory, as did CYP3A4 (Figure 10C) and CPS1(Figure 10D) expression. Furthermore, on culture days 3, 5, and 8, the levels of albumin secretion, urea synthesis, CYP3A4, and CPS1 expression were significantly elevated in PET-COL-cultured cells compared to those grown on PET scaffolds ($p < 0.001$). These results suggest that the collagen coating has the potential to modulate cellular functions, facilitating the differentiation of human hepatic progenitor HepaRG cells to acquire more mature hepatocyte-like functionalities, ultimately enhancing their albumin secretion, urea synthesis, and expression capacities of CYP3A4 and CPS1.

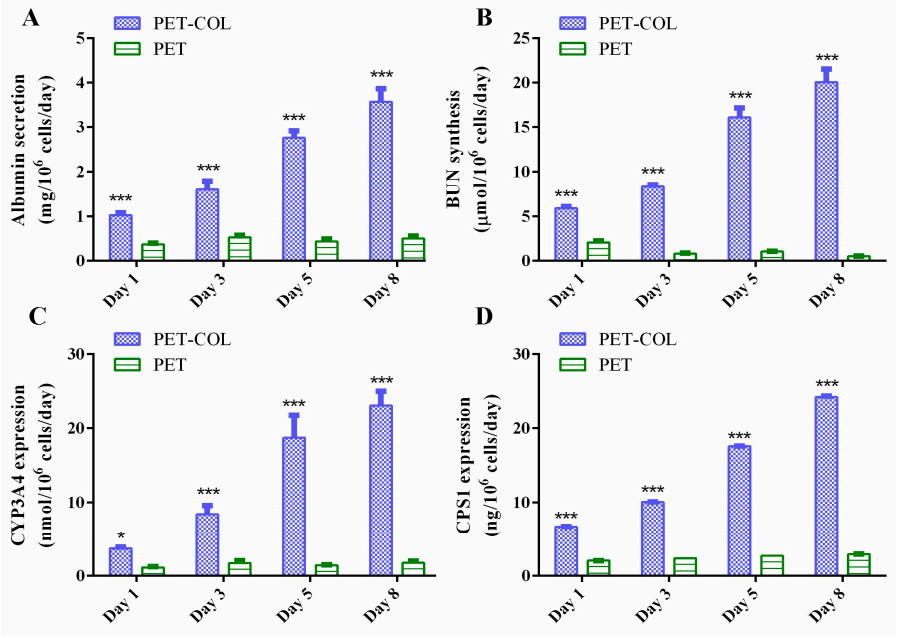

Figure 10. Cell function of HepaRG cells growing on PET and PET-COL fibers on day 1, day 3, day 5, and day 8. (**A**) Albumin secretion; (**B**) BUN synthesis; (**C**) CYP3A4 expression; (**D**) CPS1 expression. Data are mean ± SD, n = 3; *: $p < 0.05$; ***: $p < 0.001$.

4. Conclusions

This paper presents the development of a fibrous scaffold material coated with type I collagen, designated as PET-COL, utilizing PET polyester fiber as its fundamental scaffolding component. The manufacturing process encompasses the carboxylation of the PET surface, activation and crosslinking facilitated by EDC/NHS, and the subsequent coupling of collagen. Furthermore, this article delves into the characterization of the material's physicochemical properties and biological effects, with the ultimate goal of verifying its potential utility in artificial liver support systems. The obtained results indicate the following:

- FTIR analysis revealed that PET-COL displays characteristic absorption peaks of type I collagen, specifically Amid II at 1550 cm^{-1}, Amid I at 1665 cm^{-1}, and Amid A at 3330 cm^{-1}. Concurrently, the nitrogen content on the material surface amounted to 17.36%. The application of a collagen coating significantly enhanced the hydrophilicity of the material, resulting in a decrease in the water contact angle of the PET-COL scaffold from 132.97° to 74.74° ($p < 0.001$). Utilizing second harmonic generation microscopy, we visually observed the presence of a green fluorescent signal emanating from the collagen on the PET-COL surface. Furthermore, HPLC-MS analysis confirmed a collagen coating content of 33.30 μg/piece;
- The biological efficacy of the material was assessed through in vitro cell culture experiments. The outcomes indicated a substantial proliferation of HepaRG cells on the PET-COL substrate. Notably, cell viability, albumin secretion, urea synthesis, and CYP3A4 and CPS1 expression were markedly elevated compared to the untreated group ($p < 0.001$), highlighting robust biological activity. These observations implicate that the application of a collagen coating has the potential to augment the biocompatibility of PET materials, thereby facilitating cell adhesion and proliferation.

The present study integrated the stability inherent in synthetic polymer materials with the excellent biocompatibility of natural polymers, aiming to create a composite hepatocyte culture scaffold featuring a fiber structure. This scaffold promotes cell adhesion, proliferation, and differentiation, thus serving as an ideal substrate for hepatocytes cultured in bioreactors and being a promising candidate for application in bioartificial livers.

Author Contributions: Conceptualization, Y.L.; Methodology, G.Z.; Validation, S.L.; Investigation, Y.Z. and J.G.; Writing—original draft, Y.L.; Writing—review and editing, G.Z.; Supervision, Y.Z. and S.L. All authors have read and agreed to the published version of the manuscript.

Funding: This research was funded by the National Key R&D Program of China (2022YFA1104900), the National Natural Science Foundation of China (31972926).

Institutional Review Board Statement: Not applicable.

Informed Consent Statement: Not applicable.

Data Availability Statement: The data presented in this study are available on request from the corresponding author. The data are not publicly available due to privacy.

Acknowledgments: The authors would like to thank the institute of Process Engineering, Chinese Academy of Sciences, for creating the research infrastructure.

Conflicts of Interest: The authors declare no conflicts of interest.

References

1. Wu, T.; Li, J.; Shao, L.; Xin, J.; Jiang, L.; Zhou, Q.; Shi, D.; Jiang, J.; Sun, S.; Jin, L.; et al. Development of diagnostic criteria and a prognostic score for hepatitis B virus-related acute-on-chronic liver failure. *Gut* **2018**, *67*, 2181–2191. [CrossRef]
2. Kezer, C.A.; Simonetto, D.A.; Shah, V.H. Acute on Chronic Liver Failure in Patients with Alcohol-Associated Hepatitis: A Review. *Clin. Liver Dis.* **2023**, *27*, 659–670. [CrossRef]
3. Flamm, S.L.; Yang, Y.X.; Singh, S.; Falck-Ytter, Y.T. American Gastroenterological Association Institute guidelines for the diagnosis and management of acute liver failure. *Gastroenterology* **2017**, *152*, 644–647. [CrossRef]
4. Bernal, W.; McPhail, M.J. Acute liver failure. *J. Hepatol.* **2021**, *74*, 1489–1490. [CrossRef]
5. Jayalakshmi, V.T.; Bernal, W. Update on the management of acute liver failure. *Curr. Opin. Crit. Care* **2020**, *26*, 163–170. [CrossRef]
6. Kumar, B.R.V.; Sarin, S.K. Acute-on-chronic liver failure: Terminology, mechanisms and management. *Clin. Mol. Hepatol.* **2023**, *29*, 670–689.
7. Zhou, P.Q.; Zheng, S.P.; Yu, M.; He, S.S.; Weng, Z.H. Prognosis of acute-on-chronic liver failure patients treated with artificial liver support system. *World J. Gastroenterol.* **2015**, *21*, 9614–9622. [CrossRef]
8. Cardoso, L.M.; Moreira, L.F.; Pinto, M.A.; Henriques-Pons, A.; Alves, L.A. Domino Hepatocyte Transplantation: A Therapeutic Alternative for the Treatment of Acute Liver Failure. *Can. J. Gastroenterol. Hepatol.* **2018**, *2018*, 2593745. [CrossRef]
9. Kimmann, M.; Trebicka, J. Acute-On-Chronic Liver Failure: Current Interventional Treatment Options and Future Challenges. *J. Pers. Med.* **2023**, *13*, 1052. [CrossRef]
10. He, Y.T.; Qi, Y.N.; Zhang, B.Q.; Li, J.B.; Bao, J. Bioartificial liver support systems for acute liver failure: A systematic review and meta-analysis of the clinical and preclinical literature. *World J. Gastroenterol.* **2019**, *25*, 3634–3648. [CrossRef]
11. Chen, H.S.; Joo, D.J.; Shaheen, M.; Li, Y.; Wang, Y.; Yang, J.; Nicolas, C.T.; Predmore, K.; Amiot, B.; Michalak, G.; et al. Randomized trial of spheroid reservoir bioartificial liver in porcine model of posthepatectomy liver failure. *Hepatology* **2019**, *69*, 329–342. [CrossRef] [PubMed]
12. Li, P.; Liang, X.; Xu, S.; Xiong, Y.; Huang, J. A non-bioartificial liver support system combined with transplantation in HBV-related acute-on-chronic liver failure. *Sci. Rep.* **2021**, *11*, 2975. [CrossRef] [PubMed]
13. Larsen, F.S. Artificial liver support in acute and acute-on-chronic liver failure. *Curr. Opin. Crit. Care* **2019**, *25*, 187–191. [CrossRef] [PubMed]
14. Karvellas, C.J.; Subramanian, R.M. Current evidence for extracorporeal liver support systems in acute liver failure and acute-on-chroliver failure. *Crit. Care Clin.* **2016**, *32*, 439–451. [CrossRef] [PubMed]
15. Zhang, Z.; Zhao, Y.C.; Cheng, Y.; Jian, G.D.; Pan, M.X.; Gao, Y. Hybrid bioartificial liver support in cynomolgus monkeys with D-galactosamine-induced acute liver failure. *World J. Gastroenterol.* **2014**, *20*, 17399–17406. [CrossRef] [PubMed]
16. Liu, W.; Hu, D.; Gu, C.; Zhou, Y.; Tan, W.S. Fabrication and in vitro evaluation of a packed-bed bioreactor based on an optimum two-stage culture strategy. *J. Biosci. Bioeng.* **2019**, *127*, 506–514. [CrossRef] [PubMed]
17. Safakar, A.Y.; Hamel, K.M.; Mehrnezhad, A.; Jung, J.P.; Park, K. Development of rolled scaffold for high-density adherent cell culture. *Biomed. Microdevices.* **2019**, *22*, 4.
18. Pasqua, M.; Pereira, U.; Messina, A.; de Lartigue, C.; Vigneron, P.; Dubart-Kupperschmitt, A.; Legallais, C. HepaRG self-assembled spheroids in alginate beads meet the clinical needs for bioartificial liver. *Tissue Eng. Part A.* **2020**, *26*, 613–622. [CrossRef]
19. Sibuea, C.V.; Pawitan, J.A.; Antarianto, R.; Jasirwan, C.O.M.; Sianipar, I.R.; Luviah, E.; Nurhayati, R.W.; Mubarok, W.; Mazfufah, N.F. 3D Co-culture of hepatocyte, a hepatic stellate cell line, and stem cells for developing a bioartificial liver prototype. *Int. J. Technol.* **2020**, *11*, 951–962. [CrossRef]
20. Zhao, C.; Li, Y.; Peng, G.; Lei, X.; Zhang, G.; Gao, Y. Decellularized liver matrix-modified chitosan fibrous scaffold as a substrate for C3A hepatocyte culture. *J. Biomater. Sci. Polym. Ed.* **2020**, *31*, 1041–1056. [CrossRef]

21. Bélanger, M.C.; Marois, Y.; Roy, R.; Mehri, Y.; Wagner, E.; Zhang, Z.; King, M.W.; Yang, M.; Hahn, C.; Guidoin, R. Selection of a poly urethane membrane for the manufacture of ventricles for a totally implantable artificial heart: Blood compatibility and biocompatibility studies. *Artif. Organs.* **2000**, *24*, 879–888. [CrossRef] [PubMed]
22. Kolar, M.; Mozetič, M.; Stana-Kleinschek, K.; Fröhlich, M.; Turk, B.; Vesel, A. Covalent binding of heparin to functionalized PET materials for improved haemocompatibility. *Materials* **2015**, *8*, 1526–1544. [CrossRef]
23. Zheng, Z.; Ren, L.; Zhai, Z.; Wang, Y.; Hang, F. Surface modification on polyethylene terephthalate films with 2-methacryloyloxyethyl phosphorylcholine. *Mater. Sci. Eng. C. Mater. Biol. Appl.* **2013**, *33*, 3041–3046. [CrossRef]
24. Sokolsky-Papkov, M.; Agashi, K.; Olaye, A.; Shakesheff, K.; Domb, A.J. Polymer carriers for drug delivery in tissue engineering. *Adv. Drug. Deliv. Rev.* **2007**, *59*, 187–206. [CrossRef]
25. Sherman, V.R.; Yang, W.; Meyers, M.A. The materials science of collagen. *J. Mech. Behav. Biomed. Mater.* **2015**, *52*, 22–50. [CrossRef] [PubMed]
26. Huang, L.; Zhu, L.; Shi, X.; Xia, B.; Liu, Z.; Zhu, S.; Yang, Y.; Ma, T.; Cheng, P.; Luo, K.; et al. A compound scaffold with uniform longitudinally oriented guidance cues and a porous sheath promotes peripheral nerve regeneration in vivo. *Acta Biomater.* **2018**, *68*, 223–236. [CrossRef] [PubMed]
27. Nijsure, M.P.; Pastakia, M.; Spano, J.; Fenn, M.B.; Kishore, V. Bioglass incorporation improves mechanical properties and enhances cell-mediated mineralization on electrochemically aligned collagen threads. *J. Biomed. Mater. Res. A* **2017**, *105*, 2429–2440. [CrossRef]
28. Nguyen, T.U.; Bashur, C.A.; Kishore, V. Impact of elastin incorporation into electrochemically aligned collagen fibers on mechanical properties and smooth muscle cell phenotype. *Biomed. Mater.* **2016**, *11*, 025008. [CrossRef] [PubMed]
29. Du, T.; Chen, Z.; Li, H.; Tang, X.; Li, Z.; Guan, J.; Liu, C.; Du, Z.; Wu, J. Modification of collagen–chitosan matrix by the natural crosslinker alginate dialdehyde. *Int. J. Biol. Macromol.* **2016**, *82*, 580–588. [CrossRef]
30. Goissis, G.; Marcantonio Jr, E.; Marcantônio, R.A.; Lia, R.C.; Cancian, D.C.; de Carvalho, W.M. Biocompatibility studies of anionic collagen membranes with different degrees of glutaraldehyde cross-linking. *Biomaterials* **1999**, *20*, 27–34. [CrossRef]
31. Olde Damink, L.H.; Dijkstra, P.J.; van Luyn, M.J.; van Wachem, P.B.; Nieuwenhuis, P.; Feijen, J. Cross-linking of dermal sheep collagen using a water-soluble carbodiimide. *Biomaterials* **1996**, *17*, 765–773. [CrossRef]
32. Ai, C.; Cai, J.; Zhu, J.; Zhou, J.; Jiang, J.; Chen, S. Effect of PET graft coated with silkfibroin via EDC/ NHS crosslink on graft-bone healing in ACL Reconstruction. *RSC. Adv.* **2017**, *7*, 51303–51312. [CrossRef]
33. Ma, T.; Li, Y.; Yang, S.T.; Kniss, D.A. Tissue engineering human placenta trophoblast cells in 3-D fibrous matrix: Spatial effects on cell proliferation and function. *Biotechnol. Prog.* **1999**, *15*, 715–724. [CrossRef]
34. Jha, S.; Malviya, R.; Fuloria, S.; Sundram, S.; Subramaniyan, V.; Sekar, M.; Sharma, P.K.; Chakravarthi, S.; Wu, Y.S.; Mishra, N.; et al. Characterization of Microwave-Controlled Polyacrylamide Graft Copolymer of Tamarind Seed Polysaccharide. *Polymers* **2022**, *14*, 1037. [CrossRef]
35. Woźniak, A.; Smok, W.; Szewczenko, J.; Staszuk, M.; Chladek, G. Influence of Hybrid Surface Modification on Biocompatibility and Physicochemical Properties of Ti-6Al-4V ELI Titanium. *J. Funct. Biomater.* **2024**, *15*, 52. [CrossRef] [PubMed]
36. Tascher, G.; Burban, A.; Camus, S.; Plumel, M.; Chanon, S.; Le Guevel, R.; Shevchenko, V.; Van Dorsselaer, A.; Lefai, E.; Guguen-Guillouzo, C.; et al. In-depth proteome analysis highlights HepaRG cells as a versatile cell system surrogate for primary human hepatocytes. *Cells* **2019**, *8*, 192. [CrossRef]
37. Jackson, J.P.; Li, L.; Chamberlain, E.D.; Wang, H.; Ferguson, S.S. Contextualizing hepatocyte functionality of cryopreserved HepaRG cell cultures. *Drug Metab. Dispos.* **2016**, *44*, 1463–1479. [CrossRef] [PubMed]
38. Ashraf, M.N.; Asghar, M.W.; Rong, Y.; Doschak, M.R.; Kiang, T.K.L. Advanced in vitro HepaRG culture systems for xenobiotic metabolism and toxicity characterization. *Eur. J. Drug Metab. Pharmacokinet.* **2019**, *44*, 437–458. [CrossRef]
39. Rebelo, S.P.; Costa, R.; Estrada, M.; Shevchenko, V.; Brito, C.; Alves, P.M. HepaRG microencapsulated spheroids in DMSO-free culture: Novel culturing approaches for enhanced xenobiotic and biosynthetic metabolism. *Arch. Toxicol.* **2015**, *89*, 1347–1358. [CrossRef] [PubMed]
40. Natale, A.; Vanmol, K.; Arslan, A.; Van Vlierberghe, S.; Dubruel, P.; Van Erps, J.; Thienpont, H.; Buzgo, M.; Boeckmans, J.; De Kock, J.; et al. Technological advancements for the development of stem cell-based models for hepatotoxicity testing. *Arch. Toxicol.* **2019**, *93*, 1789–1805. [CrossRef]